Biosensors and Bioelectronics 260 (2024) 116406

Contents lists available at ScienceDirect

Biosensors and Bioelectronics

journal homepage: www.elsevier.com/locate/bios

MicroLOCK: Highly stable microgel biosensor using locked nucleic acids as bioreceptors for sensitive and selective detection of let-7a

Sabrina Napoletano [a,c], Edmondo Battista [d], Paolo Antonio Netti [a,b,c], Filippo Causa [a,b,c,*]

[a] Interdisciplinary Research Centre on Biomaterials (CRIB), Università degli Studi di Napoli "Federico II", Piazzale Tecchio 80, 80125, Naples, Italy
[b] Dipartimento di Ingegneria Chimica del Materiali e della Produzione Industriale (DICMAPI), University "Federico II", Piazzale Tecchio 80, 80125, Naples, Italy
[c] Center for Advanced Biomaterials for Healthcare@CRIB, Istituto Italiano di Tecnologia (IIT), Largo Barsanti e Matteucci 53, 80125, Naples, Italy
[d] Department of Innovative Technologies in Medicine & Dentistry, University "G. d'Annunzio" Chieti-Pescara, Via dei Vestini, 31, 66100, Chieti, Italy

ARTICLE INFO

Keywords:
Optical sensors
Bioreceptors
Locked nucleic acids
miRNAs
Sensitivity
Nuclease resistance

ABSTRACT

Chemically modified oligonucleotides can solve biosensing issues for the development of capture probes, antisense, CRISPR/Cas, and siRNA, by enhancing their duplex-forming ability, their stability against enzymatic degradation, and their specificity for targets with high sequence similarity as microRNA families. However, the use of modified oligonucleotides such as locked nucleic acids (LNA) for biosensors is still limited by hurdles in design and from performances on the material interface. Here we developed a fluorogenic biosensor for non-coding RNAs, represented by polymeric PEG microgels conjugated with molecular beacons (MB) modified with locked nucleic acids (MicroLOCK). By 3D modeling and computational analysis, we designed molecular beacons (MB) inserting spot-on LNAs for high specificity among targets with high sequence similarity (95%). MicroLOCK can reversibly detect microRNA targets in a tiny amount of biological sample (2 μL) at 25 °C with a higher sensitivity (LOD 1.3 fM) without any reverse transcription or amplification. MicroLOCK can hybridize the target with fast kinetic (about 30 min), high duplex stability without interferences from the polymer interface, showing high signal-to-noise ratio (up to S/N = 7.3). MicroLOCK also demonstrated excellent resistance to highly nuclease-rich environments, in real samples.

These findings represent a great breakthrough for using the LNA in developing low-cost biosensing approaches and can be applied not only for nucleic acids and protein detection but also for real-time imaging and quantitative assessment of gene targeting both *in vitro* and *in vivo*.

1. Introduction

Biosensors utilizing nucleic acids bioreceptors, where sensing is based on the measurable signal of nucleic acid hybridization, have shown considerable potential for biomedical applications (Mishra, et al., 2021; Mana et al., 2022). However, nucleic acid biosensors are still limited, because of reduced bioactivity, nonspecific signals, lack of reproducibility, and susceptibility to degradation by enzymes present in biological fluids (Lahiri et al., 2019; Chowdhury et al., 2022; Mana et al., 2022).

Recently, chemically modified nucleic acids have shown increased stability and hybridization affinity to the target. Among these modifications, locked nucleic acids (LNAs) have emerged as extremely promising for revolutionizing biomarker detection and nucleic acid therapeutics (Kulkarni et al., 2021; Kamali et al., 2023). LNAs are characterized by a ribose modified via a methylene bridge (Koshkin et al., 2001; McTigue et al., 2004a), which efficiently restricts the flexibility of the sugar ring and confers a rigid conformation. This rigidity improves affinity toward the target sequences by increasing melting temperature and reducing the entropic penalty upon hybridization. As a result, LNAs exhibit high resistance to nuclease enzymes and enhanced binding specificity (Kim et al., 2022).

Molecular beacons (MBs) are advantageous probes for biosensors due to their wide dynamic range, high signal-to-noise ratio, rapid hybridization kinetics, sensitivity, and specificity (Wang et al., 2009). However, the most recent literature on the effects of LNAs substitutions on MB oligonucleotides date to 2005 (Wang et al., 2005) and 2009 (Martinez et al., 2009). Currently, no fully developed biosensors using

* Corresponding author. Interdisciplinary Research Centre on Biomaterials (CRIB), Università degli Studi di Napoli "Federico II", Piazzale Tecchio 80, 80125, Naples, Italy.
E-mail address: filippo.causa@unina.it (F. Causa).

https://doi.org/10.1016/j.bios.2024.116406
Received 18 March 2024; Received in revised form 16 May 2024; Accepted 17 May 2024
Available online 23 May 2024

LNAs as bioreceptors for direct target analyte detection exist, mainly due to challenges in design, that may hinder target recognition or lead to unwanted interactions with biosensor components (Treasurer and Levicky, 2021; Gooding, 2023).

The application of LNAs can offers advancements across various fields, both *in vitro* and *in vivo* such as, diagnostic liquid biopsies, antisense therapies, and genome engineering, addressing concerns regarding enzyme resistance and target specificity (Wang et al., 2022a; Khvorova and Watts, 2017). For instance, for liquid biopsies, the specificity and resistance of biosensors to nuclease degradation is essential for reliable results (Shi et al., 2018), considering that the DNase activity in plasma is high (Ershova et al., 2017) and further increase in pathological conditions, such as abnormal pregnancy (Tamkovich et al., 2006).

In genome engineering, incorporating LNAs in CRISPR-RNAs (crRNAs) significantly reduces off-target effects both *in vitro* and in cells (Rozners, 2022; Cromwell et al., 2018) and LNAs modified oligonucleotides have enabled more efficient and flexible genome editing (Stojic et al., 2018; Renaud et al., 2016). As antisense agents, LNAs enhance the specificity and stability of antisense oligonucleotides like siRNAs and antimiRNAs (Bajan and Hutvagner, 2020; Nedorezova et al., 2022). LNAs modified oligonucleotides can also be extended to protein detection, for example, in developing aptamers with high efficiency and at low cost (Karlsen and Wengel, 2012; Ni et al., 2021; Pal et al., 2023).

Recent efforts have focused on integrating LNAs with sensing platforms. Wang et al. have demonstrated nanopore biosensing using LNAs, characterized by slow detection speed with low DNA input but necessitating target amplification (Wang et al., 2017), or double-strand probes for biosensing with LNAs modifications have been optimized (Vilchez Mercedes et al., 2022). However, these approaches exhibit sensitivity in the nanomolar range. Therefore, challenges persist for all biosensor types, including electrochemical, optical, piezoelectric, gravimetric, and pyroelectric (Shaver and Arroyo-Curr s, 2022a). In particular, implementing biosensors with LNAs may present drawbacks due to bioconjugation on material surfaces (Xu et al., 2022) such as molecular crowding, non-specific oligonucleotide-surface interactions, and conformational constraints that compromise hybridization efficiency and sensitivity (Ma et al., 2016; Teng and Libera, 2018; Elder et al., 2015; Rao and Grainger, 2014; Ravan et al., 2014).

Among the diverse types, optical biosensors stand out for their immunity to external disturbance, stability, and low noise in optical signals (Chen and Wang, 2020; Dey et al., 2023). Additionally, the utilization of colloidal particles for optical biosensing offers antifouling properties and a large surface area for probe bioconjugation and the hybridization process (Vinogradov, 2006; Plamper and Richtering, 2017; Agrawal and Agrawal, 2018). Recent biosensor development exploits a variety of innovative materials, such as nanoparticles, functionalized polymers, graphene, and quantum dots, enhancing sensor performance and introducing new functionalities (Singh et al., 2023; Singh et al., 2023a,b; Singh et al., 2024; Li et al., 2023; Zhang et al., 2023; Gomes et al., 2024). In such landscape, polymeric microgels, including those derived from PEG, PNIPAM, PVP, and PAA, offer distinct advantages as sensitivity, selectivity and rapid response, enabling the creation of highly sensitive and adaptable sensors for diverse applications (Wang et al., 2019; Xu et al., 2022; Li et al., 2024).

We have already developed fluorescently encoded microgels for optical biosensing using unmodified DNA-MB probes as bioreceptors (Causa et al., 2015; Caputo et al., 2019a; Napoletano et al., 2023). By immobilizing MBs with a fluorescent dye at one end and a fluorescence quencher at the opposite end on microgels, we concentrated the hybridization events on the surface of the microgel. This allowed to directly quantify the target amount in the analyzed sample by measuring the fluorescence emitted from the MBs after hybridization, without target amplification (Caputo et al., 2019a; Napoletano et al., 2023).

The let-7 family is the largest microRNA (miRNA) family discovered to date, ubiquitously expressed across human tissues (Chirshev et al., 2019). In particular, the let-7a miRNA has gained significant attention across various fields, including development and stem cell biology, aging, metabolism, and cancer (Yazarlou et al., 2021; Jiang, 2019). Notably, it has emerged as a diagnostic and prognostic biomarker for cancer precision medicine (Chen et al., 2023) and as a potent antagomir in injured peripheral nerve regeneration, indicating its suitability for both diagnostic and therapeutic applications (Su et al., 2012). However let-7a shares high sequence similarity (95%) with other family members, which poses a significant challenge for detection specificity.

Driven by the extraordinary features of LNAs and the excellent sensitivity of MBs probes conjugated to microgels, we present here the development of a highly stable and amplification-free optical biosensor for the detection of let-7a. In detail, we have developed a fluorogenic biosensor for non-coding RNAs, which consists of polymeric PEG microgels conjugated with LNAs modified MBs (MicroLOCK).

We designed and tested probes with various LNAs modifications identifying the most suitable for microgels-based detection, particularly, to investigate the effects of LNAs modifications on RNA binding and duplex conformation (Tolstrup et al., 2003a; Sim et al., 2012). Therefore, to fully understand the impact of LNAs, we carried out modeling of three-dimensional (3D) structures with and without LNAs chemical modifications of the probes. We evaluated different physical parameters such as base-pairing interactions, tertiary contacts, electrostatic interactions, and entropy, all of which can affect nucleic acid folding and structure (Zheng et al., 2009; Poppleton et al., 2020; Patro et al., 2017). In addition, we performed *in silico* molecular simulations for the analysis, reconstruction, and visualization of three-dimensional nucleic acids (Pabon-Martinez et al., 2017; Xu et al., 2016, 2019; Jo et al., 2008, 2013).

We then demonstrated the applicability of MBs probes modified with LNAs to obtain highly stable, nuclease-resistant, and binding-efficient microgel biosensors capable of detecting let-7a and distinguishing it from other components of the let-7 miRNA family, even those differing by as little as a single nucleotide. The MicroLOCK biosensor provides a useful method for sensitive, stable, and specific capture and detection of non-coding-RNAs. Furthermore, we demonstrated the use of the LNA-microgel biosensor for a one-stage hybridization assay for let-7a with single-nucleotide specificity, in the presence of a very low concentration (fM) of the target.

2. Materials and methods

2.1. DNA and LNA probes design and 3D molecular modeling analysis

The miRNA sequences were extracted from the database miRBase (https://mirbase.org/), and probes were designed accordingly by OligoAnalyzer and UNAfold tools. Thermodynamic parameters and secondary structures of the probes were evaluated by online tools, https://eu.idtdna.com/calc/analyzer/lna, and UNAfold (Fig. 1, Figs. S2A–B, Table S1 and Table S2). All probes were synthesized by Metabion and purified by high-performance liquid chromatography (HPLC). The 3D-DNA duplex structures were built as canonical A-DNA duplex models using the w3DNA server http://w3dna.rutgers.edu. the PDB files were typed using BIOVIA Discovery Studio Visualizer to add LNA residues. Molecular docking of the hybridization of each probe to the targets was performed with the graphical processing unit CHARMM GUI https://www.charmm-gui.org/(Fig. S2C and Table S3). Free energy calculations of hybridization were performed in solution using the Monte-Carlo Ion placing method, keeping the system kept at pH 7 in a water box-type rectangular.

2.2. Microgels synthesis

Microgels labeled with the ATTO532 fluorophore were synthesized via free-radical pre-precipitation polymerization as previously described (Causa et al., 2015). The microgel size, zeta potential, conductivity, and

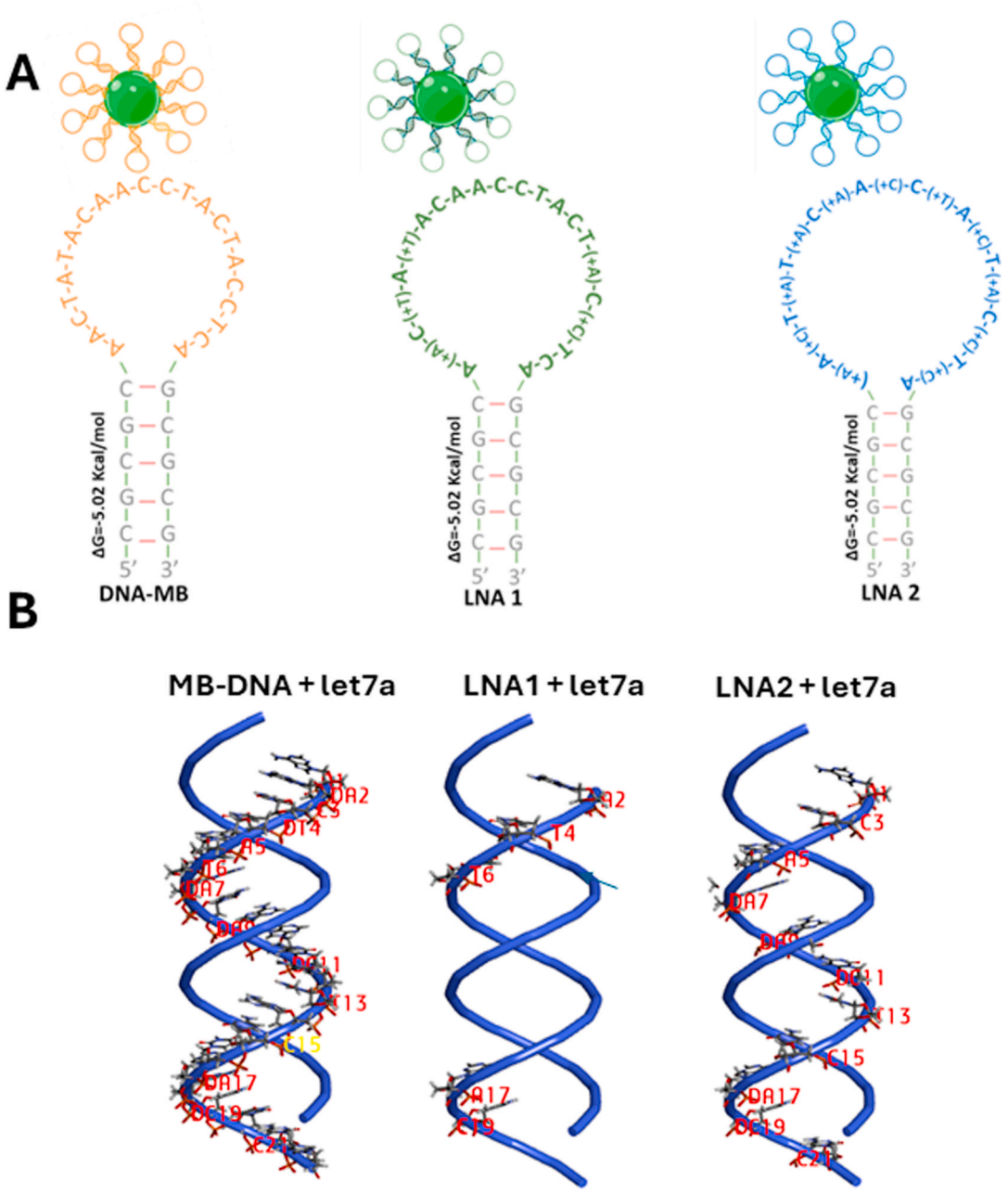

Fig. 1. (A) Secondary structures of the molecular beacon probes conjugated to microgels. (B) Tridimensional visualization of the probes-target duplexes with evidence of the modified nucleotides. DNA-MB: unmodified molecular beacon. LNA1: molecular beacon probe with LNAs modifications on the mismatch sites of let-7 family members. LNA2: molecular beacon with 50% LNA modifications.

electrophoretic mobility were characterized by dynamic light scattering (DLS) (Malvern Zetasizer Nano ZS instrument, 633 nm laser, 173° scattering angle) (Table S4). The carboxyl group content on microgels was quantified by potential titration before the bioconjugation of the MBs.

2.3. Probes bioconjugation to microgels

MBs with the dye (ATTO647N) at one end and a quencher (BBQ-650) at the opposite end were conjugated to microgels as previously described (Napoletano et al., 2023). Briefly, 1 mg of microgels in 250 μL of (2-(N-morpholino)ethanesulfonic acid) (MES) at pH 6, and MBs in 50 μL of MES pH 6 were incubated for at least 5 h. Then, the carboxylic groups on the microgel were activated using 0.5 M of the coupling agent 1-Ethyl-3-(3-dimethylaminopropyl) carbodiimide (EDC) by stirring vigorously briefly and leaving them in ice for 20 min. Subsequently, MBs solution was added to the microgels by incubating overnight at 300 rpm at 4 °C. Microgels conjugated with MBs were washed three times to remove the unreacted MBs and suspended in Tris(hydroxymethyl)aminomethane (TRIS) 0.1 M. Bioconjugation was optimized by coupling 0.25 nmol of the MB Unconjugated and conjugated microgels were characterized by DLS (dynamic light scattering). Briefly, the Z-potential and size of microgels unconjugated and conjugated with 0.25 nmol of MBs, were measured by dispersing microgels in H_2O, PBS, KCl 10^{-3} M or Tris-EDTA (pH 8) at a concentration of 50 μg/mL. A total of three runs, each comprising three cycles, were conducted.

2.4. MicroLOCK assay calibration curve

Microgels conjugated with MBs at a concentration of 0.5 μg/mL

(corresponding to 1.45 10^7 microgels) were used for the final assay by directly mixing with the target let-7a. A calibration curve was done using serial dilutions of synthetic let-7a in TE. The samples were analyzed by confocal microscopy with an objective 63× 1.40 oil (Zeiss) using lasers 543 nm and 633 nm. Lasers power and detector gains were kept constant with a scan speed of 8000 Hz. For each target concentration, 20 images were collected and analyzed by ImageJ software. The assay for each concentration of let-7a took about 1 h and was done in triplicate. Data are from 5 sets of 3 independent tests. To estimate the limit of detection (LOD), 20 replicates of the blank sample (microgels without the target) were measured. To assess the performance of both MicroLOCK and MB-DNA microgels in human serum, we conducted the assay after adding 100 pM of synthetic let-7a target.

2.5. Fluorescence plate reader assays

Microgels at the concentration of 500 μg/mL were suspended in TE and measured at room temperature before and after the addition of 100 mM NaOH, in Flat-Bottom Corning 384-Well Microplates using an EnSpire multimode plate reader (PerkinElmer). As a negative control (NC) we measured wells with buffer solution only.

2.6. Nuclease resistance

Nuclease treatment of both MicroLOCK and microgels with MB-DNA was performed using the RNase-free DNase I (Cat No 79254). For each reaction: 500 μg/mL of microgels resuspended in 87.5 μL of H_2O, 10 μL of buffer RDD, and 5 μL of DNase I enzyme (13.63 Kunitz units). All reactions were performed at 25 °C and measured with a multimodal spectrofluorometer (PerkinElmer) after 15 min. For serum stability assay, both MicroLOCK and microgels with unmodified MB-DNA were incubated at 37 °C in 100 μl of human serum type AB (male) from Sigma Aldrich. Samples were measured after 15 min.

2.7. Statistics

All results are expressed as the mean of three different experiments; each sample was tested in triplicate. Data have been analyzed using a student t-test, and only statistically significant as $p < 0.05$ were considered. For nuclease experiments a two-sample *t*-test was performed, p–value = 0.01. Error bars are the standard deviation of the data.

3. Results and discussion

3.1. MicroLOCK working mechanism

This study presents the development of MicroLOCK, a nuclease-resistant fluorogenic biosensor for non-coding RNAs, consisting of microgels conjugated with MBs modified with LNAs. MBs oligonucleotide probes consist of a fluorescent dye at one end and a fluorescence quencher at the opposite end. Upon binding to the target, the probe undergoes a conformational change, activating fluorescence following target detection. Microgels conjugated with MBs allow direct measurement of emitted light from the assay and target quantification in real-time, without prior pretreatment, purification of the target or reverse transcription and amplification. Fluorescence reading on the microgel surface can be performed using fluorescence imaging techniques. In this study, we have LNA as a bioreceptor, in which the 2′-oxygen bridged to the 4′-carbon, prevents them from adopting a zig-zag conformation and thereby increases their stability and affinity for their targets. Furthermore, LNA forms additional hydrogen bonds with the complementary

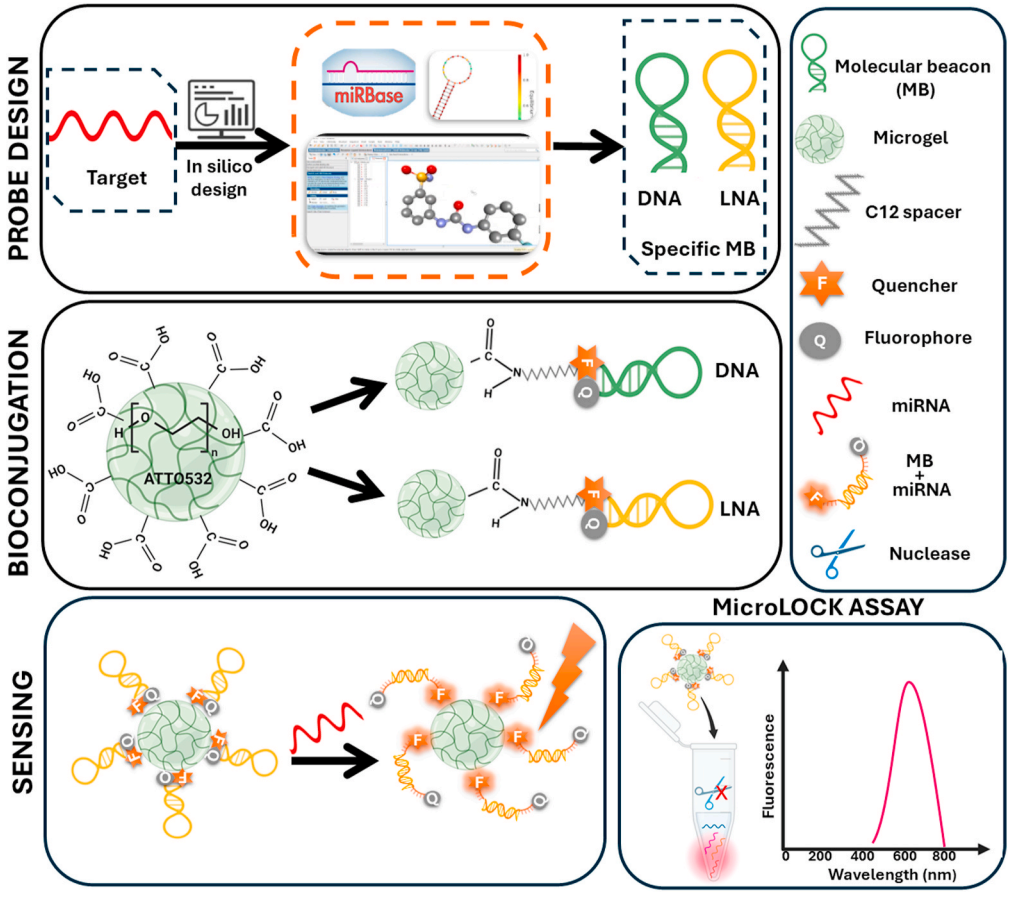

Scheme 1. Illustration of the development and working mechanism of MicroLOCK biosensor for direct, amplification-free and enzyme–free detection of microRNA.

bases in the target sequence, stabilizing the probe-target complex. The steps of MicroLOCK development and the working mechanism are depicted in Scheme 1.

3.2. Design of the one-pot LNA probe and three-dimensional hybridization analysis

LNAs follow specific design guidelines, including the positioning within a sequence, the length, and probe type (Tolstrup et al., 2003a). The effectiveness of LNA modifications depends on the specific context, such as the nucleotide sequence, the conformation, the material of the structures to which LNAs are bound, and the type of biological application.

In this study, LNAs have been strategically placed within the probe sequence. Initially, we identified positions along the target sequence where enhanced binding affinity was desirable, based on sequences of all targets of the let-7 family, showing high sequence similarity (95%) (Fig. 1 and Fig. S1). Accordingly, we have incorporated LNAs at strategic positions around the mismatch sites. Before selecting the optimal LNA bioreceptor, we have conducted *in silico* evaluations of the melting temperature (Tm) and we have assessed the formation and nature of any secondary structures. The LNAs have been strategically placed to avoid regions that may be obstructed or inaccessible due to structural constraints or interactions with other biomolecules. As shown in Fig. 1 and Table S1, we designed a MB probe with canonical bases (DNA-MB), a molecular beacon with LNA modification on the mismatch sites (LNA1), and a molecular beacon with 50% LNA-modified bases (LNA2).

3.3. In silico and experimental characterization of probe hybridization

Thermodynamic parameters were calculated considering the experimental conditions, including the concentration of the probes and salt/ionic strength of the environment (Fig. S2 and Table S2).

These values demonstrate the higher stability conferred to MBs probes by LNAs modifications. Moreover, a most favorable ΔG value increases the affinity of the probe with the target which results in the faster kinetic of hybridization of the target in solution, as we have validated through experimental assay in solution (Fig. S3).

We then tested *in silico* probes-targets duplexes stability and the duplex percentage in a range of temperatures between 0 and 100 °C, these analyses further confirmed the increased duplex stability conferred by modified LNAs probes compared to DNA unmodified probes (Fig. S4, Fig. S5, and Fig. S6). Furthermore, we studied the binding features of LNAs over unmodified MBs when forming the duplex, by thermodynamic calculations and structural 3D modeling. We calculated intermolecular interaction on 3D models of probes-targets duplexes hybridization (Fig. S2C and Table S3) demonstrating a stronger interaction of the target with LNAs probes than unmodified DNA probes. Further details are in Paragraph S1.

3.4. Effects of bioconjugation of probes to microgels

Probe density, orientation, and distance from the microgel surface are key parameters that can strongly influence the biosensor performance. Overcrowded surface coverage of the immobilized probe can lead to steric hindrance and influence the efficiency of hybridization but also the kinetics of capturing the target molecule. (Mahjour et al., 2020; Meng et al., 2023).

For the microgels biosensor development, each probe was conjugated to microgels using an optimized coupling protocol previously employed in our laboratory (Causa et al., 2015; Napoletano et al., 2023), detailed in Section 2 Materials and Methods and Scheme 1. Briefly, the microgels have been synthesized with free carboxylic groups which have been subsequently activated with EDC for the immobilization of nucleic acid bioreceptor. The coupling occurred through the formation of a peptide bond between the amine group on the oligonucleotide probe and the carboxylic acid group on the microgel.

Proper bioconjugation was assessed by measuring the fluorescence of the ATTO647N on the MB, both with and without the addition of the target, at a microgels concentration of 25 μg/mL (Fig. S7). It is worth noting that we did not observe the same results as in the solution for the hybridization of LNA2 (Fig. S3) when the probes are conjugated to the microgels. This discrepancy may be attributed to the incorrect opening of LNA2 (Fig. S7) on the microgels upon contact with the target. We hypothesize that modifying the probe with 50% of LNA modifications may confer too much rigidity, thus hindering the opening of the LNA2 once immobilized on the microgel.

Instead, for LNA1, the optimal coupling amount has been found to be 0.25 nmol, where we have observed optimal biosensor performance. This result means that, using such amount of the MB, the probes are appropriately spaced on the surface of microgels and exhibits a low background signal as shown in Fig. 3A–B (No Target signal) where we used a lower concentration of microgels 0.5 μg/mL. This minimal background signal is optimal for achieving proper probe folding, target binding, and signal transduction. Furthermore, we have demonstrated that immobilizing LNAs on microgels surfaces supports a higher signal-to-noise ratio compared to microgels traditionally prepared with unmodified MBs and a lower background in the absence of the target (Fig. 3A–B).

3.5. – MBs reversibility on MicroLOCK

The reversibility of MBs conformational changes is a crucial aspect of biosensor reusability. We tested the correct opening and reversibility of both LNA1 and MB-DNA probes once immobilized on the microgel surface. Verifying the correct opening and closing of MBs on the surface of microgels, particularly in response to temperature changes, is crucial to evaluating functional performances. Verifying that conformational changes occur correctly ensures that the biosensor functions as intended, providing reliable and accurate detection of the target analyte. We have done this evaluation by measuring fluorescence over a temperature range from 25 °C to 95 °C (refer to Fig. 2). After reaching 95 °C, we returned the temperature to 25 °C to observe whether the MB could return to its closed state. These results demonstrate that we designed the MB with spot-on LNA modifications that can hybridize the target upon bioconjugation to microgels without constraint due to the bioconjugation or interferences from the material surface. These data confirm the stability and functionality of the biosensor across diverse temperature conditions. Furthermore, they ensure that the properties of the microgels do not interfere with the function of the MB-based biosensor. These results open the way to future experiments for optimizing regeneration protocols and demonstrate the reusability of MicroLOCK.

3.6. Analytical performance of MicroLOCK biosensor

Following preliminary characterizations, calibrations were conducted to determine the limit of detection (LOD) and the dynamic range of MicroLOCK and to compare it with microgels conjugated with MB-DNA (Fig. 3). We found that MicroLOCK can detect let-7a with high sensitivity as the LOD was calculated to be 1.3 fM (Fig. 3A and Fig. S9). In contrast, microgels conjugated with MB-DNA exhibit lower sensitivity, with a LOD of 3.7 fM (Fig. 3B and Fig. S9). The higher sensitivity of MicroLOCK is also attributed to its lower fluorescence background (Fig. 3A–B), resulting in a high signal to noise ratio (S/N = 7.3).

Moreover, MicroLOCK shows improved performance in the detection of let-7a in human serum without sample pretreatment or RNA purification. At a concentration of 100 pM, the fluorescence value of MicroLOCK closely matches that measured in saline buffer at the same concentration (100 pM). In contrast, a greater deviation is observed for the fluorescence of the microgel with MB-DNA in serum compared to the measurement in saline buffer (Fig. 3C). We can speculate that the more

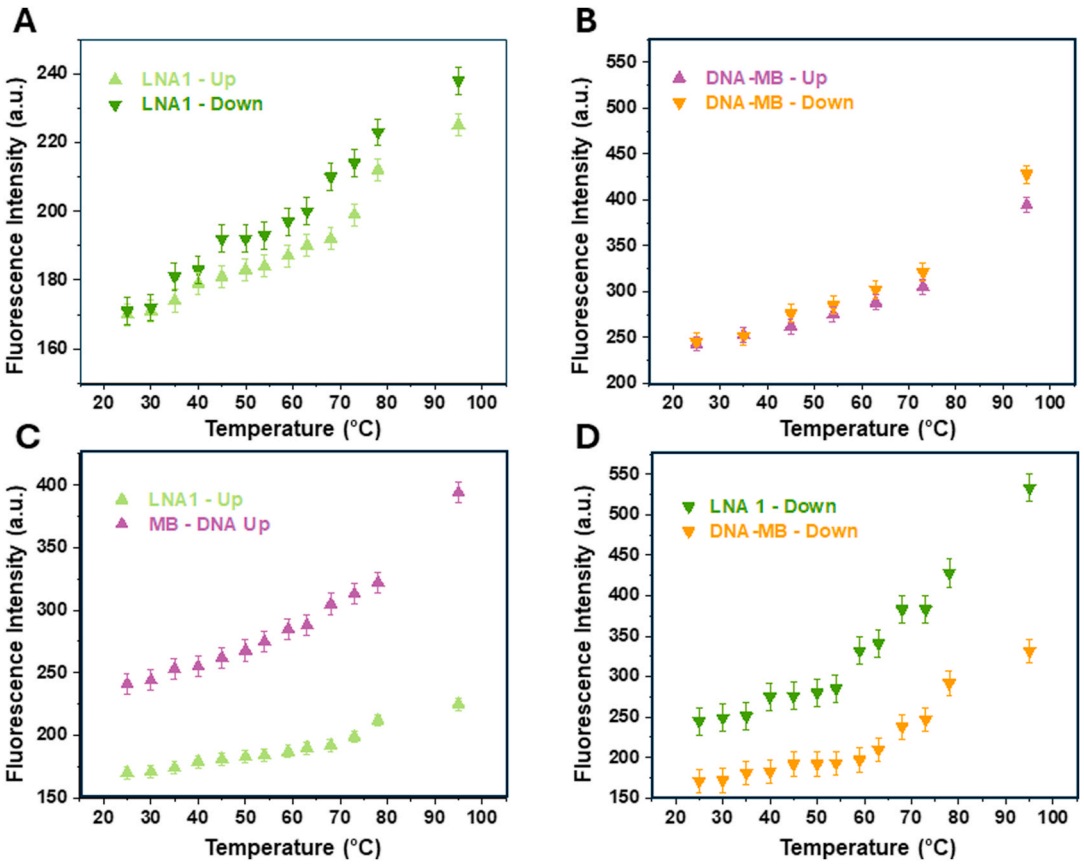

Fig. 2. MicroLOCK reversibility. (A) Fluorescence measurement of MicroLOCK bringing the temperature Up and Down (25 °C–95 °C). (B) Fluorescence measurement of MB-DNA on microgels bringing the temperature Up and Down (25 °C–95 °C). (C) Comparison of fluorescence measurement of microgels conjugated with MB-DNA and MicroLOCK during a temperature ramp from 25 °C to 95 °C (Up). (D) Comparison of fluorescence measurement of microgels conjugated with MB-DNA and MicroLOCK during a temperature ramp from 95 °C to 25 °C (Down). LNA1: MicroLOCK. MB-DNA: microgels with unmodified molecular beacons. The results of each temperature point represent the mean of three different technical replicates. Error bars are SD (standard deviation) of the data from the mean.

rigid backbone of the probe used to develop MicroLOCK may support a more upright open backbone structure, thereby increasing the affinity for the target. Indeed, as reported in Fig. 3E, there is enhanced stability observed in the duplex formed by the target and the LNA compared to the conventional MB probe. This stability is beneficial for preventing nonspecific interactions of the LNA1 capture probes with the underlying solid surface of the microgel and avoiding unspecific signals. A schematic workflow illustrating how the assay with MicroLOCK is conducted is depicted in Fig. 3D and Scheme 1.

Three different replicates were tested for each concentration; the results represent the mean of three different technical replicates for each sample. Error bars are SD (standard deviation) of the data from the mean.

3.7. Nuclease resistance

Most importantly, we observed the resistance of MicroLOCK to the action of nuclease enzymes by treatment with DNAase I (90 U/mL) for 15 min (Fig. 4A). Nuclease resistance was monitored by fluorescence measurement assuming that the increased fluorescence without the target is due to the hydrolysis of the nucleotide chain that releases the fluorophore in solution. We compared these results with the maximum opening measured after the addition of sodium hydroxide (NaOH) (Fig. S8). We demonstrate that MicroLOCK is more resistant to the action of nuclease enzymes than microgels conjugated with MB-DNA.

We observe a 42% increase in optical signal for MB-DNA between treated and untreated, which is statistically significant. In contrast, only a 10% increase for LNA1 shows a non-statistically significant difference (Fig. 4A). MicroLOCK also demonstrates enhanced resistance to nucleases in human serum, both at room temperature and at the physiological temperature of 37 °C (Fig. 4B). We can explain this nuclease resistance since LNAs contain a methylene bridge that connects the 2′-oxygen and 4′-carbon of the ribose sugar in the nucleotide. This modification hinders the accessibility of nucleases to the phosphodiester bonds in the backbone, making LNAs more resistant to degradation by nucleases. Additionally, LNAs exhibit enhanced binding affinity to their target sequences, which can further contribute to their resistance to nuclease degradation. Although the nuclease resistance of LNAs has been reported in the literature, it has never been evaluated with this sequence and with these particular modifications. Especially here, we demonstrate that this property is preserved even when the LNA probe is immobilized and in contact with the material of the microgel.

3.8. MicroLOCK performances in real samples

The performance of biosensors necessitates defining the limit of detection (LOD), especially in complex biological samples (Masson, 2020). The matrix effect commonly interferes negatively with analyte detection, reducing sensor sensitivity. A common strategy to address this issue is sample dilution, but it does not accurately reflect realistic conditions and further reduces analyte concentration, particularly in cases involving low concentrations such as circulating biomarkers for liquid biopsies. An ideal sensor should effectively perform in pure real samples without dilution or processing (Li et al., 2017). We have previously evaluated the antifouling properties of the microgels used in developing the MicroLOCK biosensor (Causa et al., 2015; Caputo et al., 2019a;

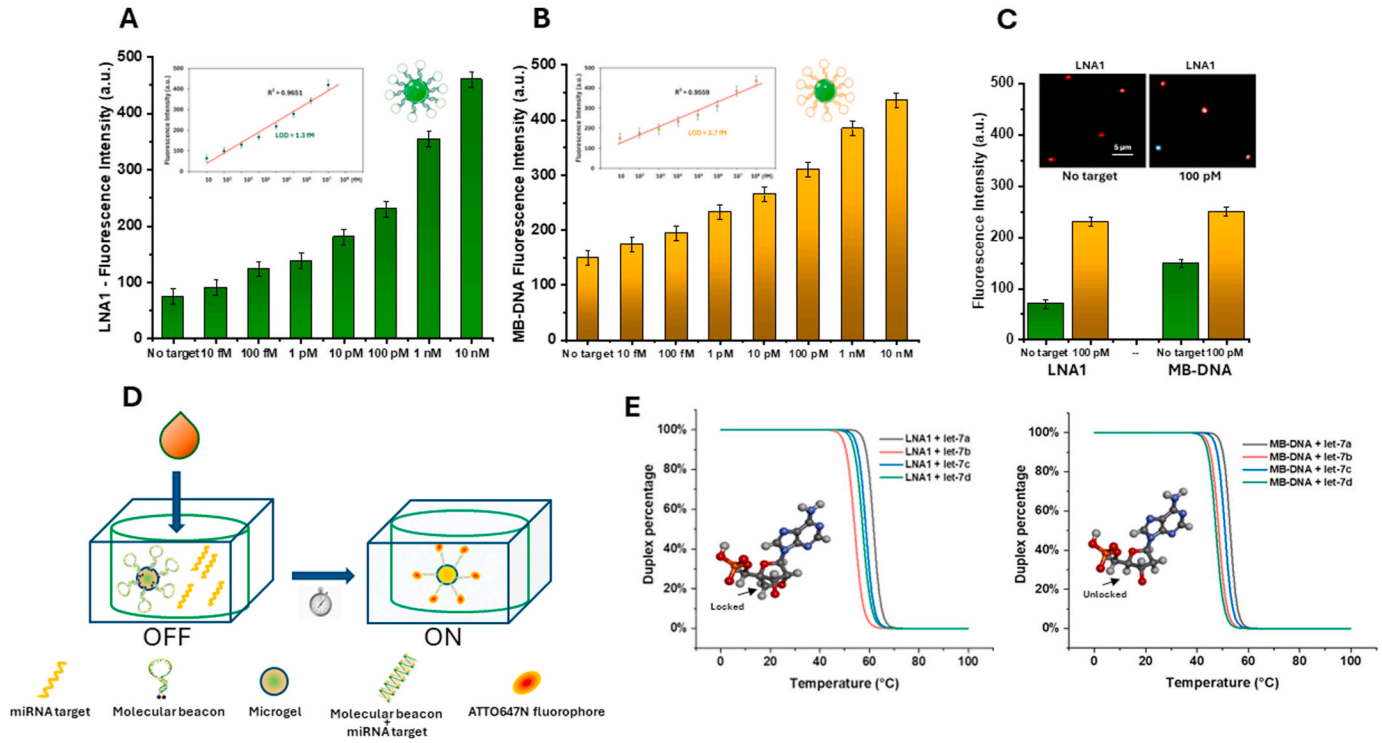

Fig. 3. Performance of MicroLOCK in detecting let-7a serial dilutions (10 fM – 10^6 fM) in Tris-EDTA (TE). (A) MicroLOCK (microgel concentration 0.5 μg/mL), inset: a small graph depicting the linear regression and reporting the limit of detection (LOD = 1.3 fM). (B) Microgels conjugated with MB-DNA, inset: a small graph showing the linear regression and reporting the limit of detection (LOD = 3.7 fM). The dose-response curves used to calculate the LOD is further reported in Fig. S8 LNA1: MicroLOCK. MB-DNA: microgels with unmodified molecular beacons (microgel concentration 0.5 μg/mL). (C) Comparison of MicroLOCK and MB-DNA performances in human serum, the confocal image within the graph represents the microgels conjugated with the LNA1 probe (MicroLOCK) in the absence (No target) and in the presence of the target (100 pM), red color in the No target image is ATTO532 fluorophore (microgel) while in the 100 pM there is the merge between ATTO532 and ATTO647N fluorophore (microgel + molecular beacon). (D) Schematic illustration of the MicroLOCK assay for miRNA detection. (E) Simulation of LNA1+let-7 and MB-DNA + let-7 targets duplex stability. Duplex percentage analyses were performed using https://eu.idtdna.com/calc/analyzer/lna. LNA1 is a MB probe with LNA modification on the mismatch sites. The molecule in the graph represents nucleotides modified via a methylene bridge (Locked ribose) and with unmodified ribose (Deoxyribose). DNA: deoxyribonucleic acid. MB: molecular beacon. LNA: locked nucleic acid. Let-7a, let-7b, let-7c, and let-7d are the targets of the various components of the let-7 family; sequences are shown in Fig. S1.

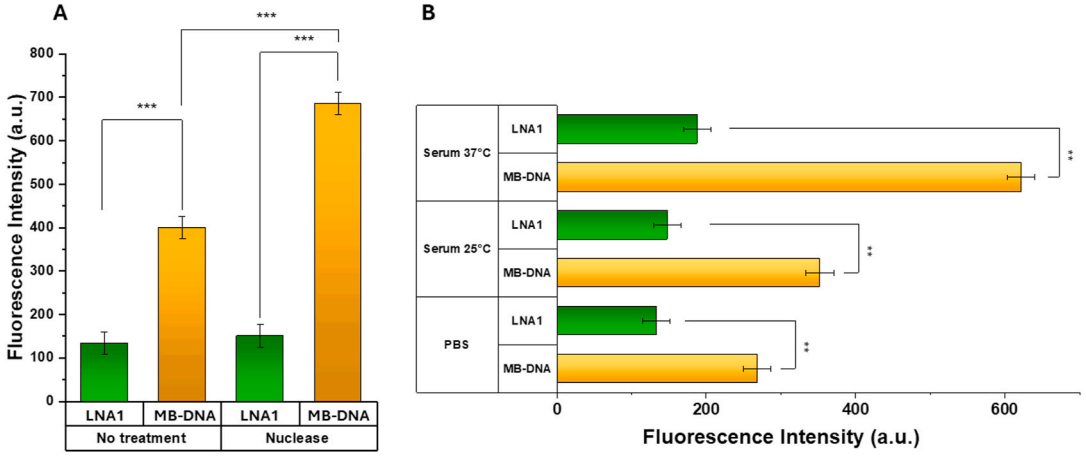

Fig. 4. MicroLOCK nuclease resistance. Values of fluorescence of MicroLOCK after treatment with nuclease enzyme. LNA1: MicroLOCK (microgels at 500 μg/mL concentration). MB-DNA: microgels with unmodified molecular beacons (microgels at 500 μg/mL concentration). No treatment: without nuclease. Nuclease: after treatment with nucleases for 15 min. Three different replicates were tested for each concentration; the results represent the mean of three different technical replicates for each sample. Two-samples *t*-test was done to reveal significant differences between MicroLOCK. Paired *t*-test was done to reveal significant differences between treated and untreated MicroLOCK and MB-DNA Error bars are SD (standard deviation) of the data from the mean. ***p-value <0,0001.

Napoletano et al., 2023). In this study, we conducted tests to verify MicroLOCK sensitivity (fM) in real biological samples, maintaining selectivity without interference from other miRNAs. The assay demonstrates stability and maintains detection capability in serum samples without pretreatment or dilution, as shown in Figs. 3C and 4B. In complex environments like serum samples, the microgel assay selectively identifies the miRNA target due to advanced stability, specificity, and high microgel antifouling properties.

3.9. MicroLOCK shelf-life and stability

The MicroLOCK biosensor, designed for practical applications involving storage and transportation, exhibits remarkable stability attributed to its key components. Incorporating stable materials such as PEG and the ATTO647N fluorophore, like the MB modified with locked nucleic acid (LNA), ensures robustness. LNAs, known for their stability and specificity, extend the bioreceptor's functional lifespan by enhancing resistance to degradation. The stability of the peptide bond bioconjugation further fortifies the structural integrity of the biosensors, Fig. S10 illustrates the biosensor's sustained performance over one month. Overall, the MicroLOCK biosensor demonstrates longevity and reliability, offering promising prospects for various practical applications. The data reported in Fig. S10 and Fig. S11, show how the MicroLOCK biosensor maintains excellent stability and how it retains the capability to detect the target even after being stored under storage conditions (4 °C) for up to one month.

3.10. MicroLOCK specificity

Finally, to test the specificity of MicroLOCK, we performed detection experiments with various targets of the let-7 family at 100 pM concentrations for both MicroLOCK and MB-DNA microgels demonstrating the higher efficiency of MicroLOCK in discriminating let-7a from the other components of the let-7 family (Fig. 5A-B-C). These data are the great breakthrough of this work, compared to previous publications, and open the way to the potential use of microgels conjugated with LNAs not only for bioanalytical purposes but also for therapeutic *in vivo* applications

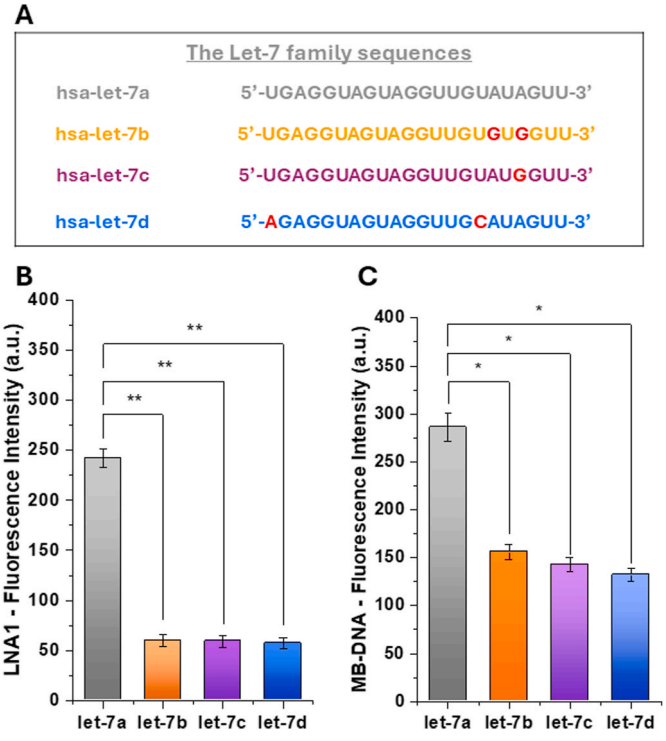

Fig. 5. MicroLOCK specificity. Fluorescence values of the assay in the presence of the let-7 family targets. (A) Sequences of mature let-7 family members (B) MicroLOCK. (C) Microgels with MB-DNA probes. LNA1: MicroLOCK. MB-DNA: microgels with unmodified molecular beacons. Three different replicates were tested for each concentration; the results represent the mean of three different technical replicates for each sample. Error bars are the SD (standard deviation) of the data from the mean. Two-samples *t*-test was done to reveal significant differences between MicroLOCK and MB-DNA. The calculated p-values ≤ 0.01**, indicating statistical significance for MicroLOCK and p-values ≤ 0.05* for MB-DNA.

Future directions for the MicroLOCK biosensor could involve several enhancements to further optimize its performance and expand its utility. One effort could be to increase sensitivity by exploring novel strategies such as incorporating fluorophores with higher quantum efficiency or selecting more efficient fluorophore-quencher pairs.

Expanding the application of the MicroLOCK biosensor beyond microRNAs presents another promising opportunity. By adapting the biosensor's design and probe sequences, it could potentially be tailored to detect a broader range of targets, including proteins, nucleic acids, or small molecules, using the bioconjugation method described in this paper. This expansion would significantly broaden its applicability in various fields, such as diagnostics, therapeutics, and environmental monitoring.

The MicroLOCK biosensor is easily integrable with emerging technologies like microfluidics or wearable devices, enhancing its portability, user-friendliness, and scalability, enabling rapid on-site detection in various settings. Its significant scalability and potential cost-effectiveness stem from miniaturization and mass production capabilities via advanced techniques such as microfluidics. This results in lower unit production costs due to reduced material consumption and the use of low-cost reagents, as the process is enzyme-free, (see Table S5) (Li et al., 2019; Pu et al., 2021; Yang et al., 2022; Nie et al., 2023, 2024). With reduced material needs and potential integration into existing diagnostic platforms, this biosensor holds promise for significant impact in clinical settings, improving access to diagnoses and enabling more efficient remote monitoring.

4. Conclusions

In conclusion, in this work, we have developed a highly sensitive and nuclease-resistant optical biosensor for the detection of non-coding RNAs. MicroLOCK utilizes PEG-based microgel polymers conjugated with MB modified with LNAs, representing a significant advancement in biosensors for miRNA detection. MicroLOCK successfully employs one-pot LNA modification which have proven to be highly effective. Notably, MicroLOCK achieves remarkable sensitivity detecting targets at a concentration as low as 1.3 fM, while also exhibiting fluorescence reversibility. Moreover, it demonstrates exceptional specificity, distinguishing targets with high sequence similarity. Excellent discrimination of let-7a from other components of the same family was obtained by rational design of LNA modifications on MB. After effective bioconjugation on the microgel interface, we also demonstrate the enhanced binding stability and nuclease resistance of MicroLOCK. Moreover, our biosensor is ready to use without complicated and time-consuming operations for RNA extraction, reverse transcription and amplification. Additionally, it does not require the use of enzymes, is low-cost, it is easy to store, further enhancing its practicality and convenience.

These findings candidate MicroLOCK as a new tool in biosensing for a wide range of bioanalytical and therapeutic applications.

Its high sensitivity and specificity make it ideal for early and accurate detection of biomarkers, such as let-7a, in medical diagnostics. Additionally, the nuclease resistance and stability of LNA-modified probes suggest their potential therapeutic use in targeted drug delivery or gene therapy contexts. The MicroLOCK biosensor holds promise for real-time imaging and precise gene targeting, both *in vitro* and *in vivo*, enabling dynamic monitoring of cellular processes like RNA dynamics. Moreover, its quantitative gene targeting capability allows for accurate gene expression analysis and manipulation in cell cultures or tissues, as well as non-invasive imaging of gene expression patterns in live animals for therapeutic modulation.

Funding sources

Financial support from the AIRC (Fondazione Italiana per la Ricerca sul Cancro – A.I.R.C.), Grant IG 2020 n. 24 623.

CRediT authorship contribution statement

Sabrina Napoletano: Writing – review & editing, Writing – original draft, Methodology, Investigation, Formal analysis, Data curation. **Edmondo Battista:** Methodology, Formal analysis, Data curation. **Paolo Antonio Netti:** Writing – review & editing, Formal analysis. **Filippo Causa:** Writing – review & editing, Writing – original draft, Validation, Supervision, Funding acquisition, Conceptualization.

Declaration of competing interest

The authors declare that they have no known competing financial interests or personal relationships that could have appeared to influence the work reported in this paper.

Data availability

Data will be made available on request.

Appendix A. Supplementary data

Supplementary data to this article can be found online at https://doi.org/10.1016/j.bios.2024.116406.

References

Agrawal, G., Agrawal, R., 2018. Small 14 (39), e1801724.
Bajan, S., Hutvagner, G., 2020. Cells 9 (1).
Caputo, T.M., Battista, E., Netti, P.A., Causa, F., 2019. ACS Appl. Mater. Interfaces 11 (19), 17147–17156.
Causa, F., Aliberti, A., Cusano, A.M., Battista, E., Netti, P.A., 2015. J. Am. Chem. Soc. 137 (5), 1758–1761.
Chen, C., Wang, J., 2020. Optical biosensors: an exhaustive and comprehensive review. Analyst 145 (5), 1605–1628.
Chen, Q.Q., Liu, Q.Y., Wang, P., Qian, T.M., Wang, X.H., Yi, S., Li, S.Y., 2023. Neural Regen Res 18 (7), 1584–1590.
Chirshev, E., Oberg, K.C., Ioffe, Y.J., Unternaehrer, J.J., 2019. Clin. Transl. Med. 8 (1), 24.
Chowdhury, S., Wang, J., Nuccio, S.P., Mao, H., Di Antonio, M., 2022. Nucleic Acids Res. 50 (13), 7247–7259.
Cromwell, C.R., Sung, K., Park, J., Krysler, A.R., Jovel, J., Kim, S.K., Hubbard, B.P., 2018. Nat. Commun. 9 (1), 1448. https://doi.org/10.1038/s41467-018-03927-0.
Dey, S., Dolci, M., Zijlstra, P., 2023. ACS Phys. Chem. Au 3 (2), 143–156.
Elder, R.M., Pfaendtner, J., Jayaraman, A., 2015. Biomacromolecules 16 (6), 1862–1869.
Ershova, E., Sergeeva, V., Klimenko, M., Avetisova, K., Klimenko, P., Kostyuk, E., Veiko, N., Veiko, R., Izevskaya, V., Kutsev, S., Kostyuk, S., 2017. Biomed Rep 7 (4), 319–324.
Gomes, H.C., Liu, X., Fernandes, A., Moreirinha, C., Singh, R., Kumar, S., Costa, F., Santos, N., Marques, C., 2024. Sensors and Actuators Reports, 7, 100186.
Gooding, J., 2023. ACS Sens. 8 (1), 1–2.
Jiang, S., 2019. Transl Oncol 12 (7), 1005–1013.
Jo, S., Kim, T., Iyer, V.G., Im, W., 2008. J. Comput. Chem. 29 (11), 1859–1865.
Jo, S., Jiang, W., Lee, H.S., Roux, B., Im, W., 2013. J. Chem. Inf. Model. 53 (1), 267–277.
Kamali, M.J., Salehi, M., Fatemi, S., Moradi, F., Khoshghiafeh, A., Ahmadifard, M., 2023. Exp. Cell Res. 423 (1), 113442.
Karlsen, K.K., Wengel, J., 2012. Nucleic acid. Ther 22 (6), 366–370.
Khvorova, A., Watts, J.K., 2017. Nat. Biotechnol. 35 (3), 238–248. https://doi.org/10.1038/nbt.3765.
Kim, H.J., Black, M., Edwards, R.A., Peillard-Fiorente, F., Panigrahi, R., Klingler, D., Eidelpes, R., Zeindl, R., Peng, S., Su, J., Omar, A.R., MacMillan, A.M., Kreutz, C., Tollinger, M., Charpentier, X., Attaiech, L., Glover, J.N.M., 2022. Nat. Commun. 13 (1), 7076.
Kulkarni, J.A., Witzigmann, D., Thomson, S.B., Chen, S., Leavitt, B.R., Cullis, P.R., van der Meel, R., 2021. Nat. Nanotechnol. 16 (7), 841.
Li, H., Dauphin-Ducharme, P., Ortega, G., Plaxco, K.W., 2017. J. Am. Chem. Soc. 139, 11207–11213.
Li, Y., Li, X., Meng, Y., Hun, X., 2019. Biosens. Bioelectron. 130, 269–275.
Li, G., Li, X., Singh, R., Zhang, G., Zhang, B., Kumar, S., 2023. Opt Lett. 48 (18), 4745–4748.
Li, L., Wang, T., Zhong, Y., Li, R., Deng, W., Xiao, X., Xu, Y., Zhang, J., Hu, X., Wang, Y., 2024. J. Mater. Chem. B 12 (5), 1168–1193.
Ma, Y., Dai, X., Hong, T., Munk, G.B., Libera, M., 2016. Analyst 142 (1), 147–155.
Mahjour, B., Shen, Y., Liu, W., Cernak, T., 2020. Nature 580 (7801), 71–75.
Mana, T., Bhattacharya, B., Lahiri, H., Mukhopadhyay, R., 2022a. XNAs: a troubleshooter for nucleic acid sensing. ACS Omega 7 (18), 15296–15307.
Mana, T., Kundu, J., Lahiri, H., Bera, S., Kolay, J., Sinha, S., Mukhopadhyay, R., 2022c. RSC Adv. 12 (15), 9263–9274.
Martinez, K., Estevez, M.C., Wu, Y., Phillips, J.A., Medley, C.D., Tan, W., 2009. Anal. Chem. 81 (9), 3448–3454.
Masson, J.F., 2020. ACS Sens. 5 (11), 3290–3292.
McTigue, P.M., Peterson, R.J., Kahn, J.D., 2004. Biochemistry 43 (18), 5388–5405.
Meng, X., O'Hare, D., Ladame, S., 2023. Biosens Bioelectron. Oct 1 237, 115440.
Mishra, S., Jeon, J., Kang, J.K., Song, S.H., Kim, T.Y., Ban, C., Choi, H., Kim, Y., Kim, M., Park, J.W., 2021. Nano Lett. 21 (21), 9061–9068.
Napoletano, S., Battista, E., Martone, N., Netti, P.A., Causa, F., 2023. Talanta 259, 124468.
Nedorezova, D.D., Dubovichenko, M.V., Belyaeva, E.P., Grigorieva, E.D., Peresadina, A. V., Kolpashchikov, D.M., 2022. Theranostics 12 (16), 7132–7157.
Ni, S., Zhuo, Z., Pan, Y., Yu, Y., Li, F., Liu, J., Wang, L., Wu, X., Li, D., Wan, Y., Zhang, L., Yang, Z., Zhang, B.T., Lu, A., Zhang, G., 2021. ACS Appl. Mater. Interfaces 13 (8), 9500–9519.
Nie, L., Zeng, X., Hongbo, L., Wang, S., Lu, Z., Yu, R., 2023. Anal. Chim. Acta 1269, 341392.
Nie, L., Zeng, X., Li, H., Wang, S., Yu, R., 2024. Talanta 266 (Pt 1), 125023.
Pabon-Martinez, Y.V., Xu, Y., Villa, A., Lundin, K.E., Geny, S., Nguyen, C.H., Pedersen, E. B., Jørgensen, P.T., Wengel, J., Nilsson, L., Smith, C.I.E., Zain, R., 2017. Sci. Rep. 7 (1), 11043.
Pal, R., Deb, I., Sarzynska, J., Lahiri, A., 2023. J. Biomol. Struct. Dyn. 41 (6), 2221–2230.
Patro, L.P.P., Kumar, A., Kolimi, N., Rathinavelan, T., 2017. J. Mol. Biol. 429 (16), 2438–2448.
Plamper, F.A., Richtering, W., 2017. Acc. Chem. Res. 50 (2), 131–140.
Poppleton, E., Bohlin, J., Matthies, M., Sharma, S., Zhang, F., Šulc, P., 2020. Nucleic Acids Res. 48 (12), e72.
Pu, J., Liu, M., Li, H., Liao, Z., Zhao, W., Wang, S., Zhang, Y., Yu, R., 2021. Talanta 230, 122158.
Rao, A.N., Grainger, D.W., 2014. Biomater. Science 2 (4), 436–471.
Ravan, H., Kashanian, S., Sanadgol, N., Badoei-Dalfard, A., Karami, Z., 2014. Anal. Biochem. 444 (1), 41–46.
Renaud, J.B., Boix, C., Charpentier, M., De Cian, A., Cochennec, J., Duvernois-Berthet, E., Perrouault, L., Tesson, L., Edouard, J., Thinard, R., Cherifi, Y., Menoret, S., Fontani re, S., de Croz, N., Fraichard, A., Sohm, F., Anegon, I., Concordet, J.P., Giovannangeli, C., 2016. Cell Rep. 14 (9), 2263–2272.
Rozners, E., 2022. J. Am. Chem. Soc. 144 (28), 12584–12594.
Shaver, A., Arroyo-Curr s, N., 2022. Curr. Opin. Electrochem. 32.
Shi, S., Ang, E.L., Zhao, H., 2018. J. Ind. Microbiol. Biotechnol. 45 (7), 491–516.
Sim, A.Y., Minary, P., Levitt, M., 2012. Curr. Opin. Struct. Biol. 22 (3), 273–278.
Singh, R., Kumar, S., Bera, S., Bhunia, S.K., 2023. ACS Appl. Nano Mater. 6 (21), 19526–19550.
Singh, R., Wang, Z., Marques, C., Min, R., Zhang, B., Kumar, S., 2023a. Biosens. Bioelectron. 236, 115424.
Singh, R., Zhang, W., Liu, X., Zhang, B., Kumar, S., 2023b. Biomed. Opt Express 14 (9), 4660–4676.
Singh, R., Zhang, W., Liu, X., Zhang, B., Kumar, S., 2024. Opt Laser. Technol. 171, 110357.
Stojic, L., Lun, A.T.L., Mangei, J., Mascalchi, P., Quarantotti, V., Barr, A.R., Bakal, C., Marioni, J.C., Gergely, F., Odom, D.T., 2018. Nucleic Acids Res. 46 (12), 5950–5966.
Su, J.L., Chen, P.S., Johansson, G., Kuo, M.L., 2012. MicroRNA 1 (1), 34–39. https://doi.org/10.2174/2211536611201010034.
Tamkovich, S.N., Cherepanova, A.V., Kolesnikova, E.V., Rykova, E.Y., Pyshnyi, D.V., Vlassov, V.V., Laktionov, P.P., 2006. Ann. N. Y. Acad. Sci. 1075, 191–196.
Teng, F., Libera, M., 2018. Langmuir 34 (49), 14969–14974.
Tolstrup, N., Nielsen, P.S., Kolberg, J.G., Frankel, A.M., Vissing, H., Kauppinen, S., 2003. Nucleic Acids Res. 31 (13), 3758–3762.
Treasurer, E., Levicky, R., 2021. J. Phys. Chem. B 125 (11), 2976–2986.
Vilchez Mercedes, S.A., Eder, I., Ahmed, M., Zhu, N., Wong, P.K., 2022. Analyst 147 (4), 722–733.
Vinogradov, S.V., 2006. Curr. Pharmaceut. Des. 12 (36), 4703–4712.
Wang, L., Yang, C.J., Medley, C.D., Benner, S.A., Tan, W., 2005. J. Am. Chem. Soc. 127 (45), 15664–15665.
Wang, K., Tang, Z., Yang, C.J., Kim, Y., Fang, X., Li, W., Wu, Y., Medley, C.D., Cao, Z., Li, J., Colon, P., Lin, H., Tan, W., 2009. Angew Chem. Int. Ed. Engl. 48 (5), 856–870.
Wang, Y., Tian, K., Shi, R., Gu, A., Pennella, M., Alberts, L., Gates, K.S., Li, G., Fan, H., Wang, M.X., Gu, L.Q., 2017. ACS Sens. 2 (7), 975–981.
Wang, Y., Guo, L., Dong, S., Cui, J., Hao, J., 2019. Adv. Colloid Interface Sci. 266, 1–20.
Wang, F., Li, P., Chu, H.C., Lo, P.K., 2022. Biosensors 12 (2).
Xu, Y., Vanommeslaeghe, K., Aleksandrov, A., MacKerell, A.D., Nilsson, L., 2016. J. Comput. Chem. 37 (10), 896–912.
Xu, Y., Gissberg, O., Pabon-Martinez, Y.V., Wengel, J., Lundin, K.E., Smith, C.I.E., Zain, R., Nilsson, L., Villa, A., 2019. PLoS One 14 (2), e0211651.
Xu, Y., Zhu, H., Denduluri, A., Ou, Y., Erkamp, N.A., Qi, R., Shen, Y., Knowles, T.P.J., 2022. Small 18 (34), e2200180.
Yang, Y.T., Liu, J.L., Sun, M.F., Yuan, R., Chai, Y.Q., 2022. Anal. Chem. 94 (18), 6874–6881.
Yazarlou, F., Kadkhoda, S., Ghafouri-Fard, S., 2021. Biomed. Pharmacother. 144, 112334.
Zhang, G., Singh, R., Zhang, B., Kumar, S., Li, G., 2023. Biomed. Opt Express 14 (11), 6100–6113.
Zheng, G., Lu, X.J., Olson, W.K., 2009. Web server issue). Nucleic Acids Res. 37, W240–W246.